

Upper critical fields in $\text{Ba}_2\text{Ti}_2\text{Fe}_2\text{As}_4\text{O}$ single crystals: Evidence for dominant Pauli paramagnetic effect

HPSTAR
516-2018

M. Abdel-Hafiez,^{1,2,3,*} J. Brisbois,⁴ Z. Zhu,⁵ A. Adamski,¹ A. Hassen,³ A. N. Vasiliev,^{6,7,8} A. V. Silhanek,⁴ and C. Krellner¹

¹*Institute of Physics, Goethe University Frankfurt, 60438 Frankfurt am Main, Germany*

²*Center for High Pressure Science and Technology Advanced Research, Beijing 100094, China*

³*Physics Department, Faculty of Science, Fayoum University, 63514-El Fayoum, Egypt*

⁴*Experimental Physics of Nanostructured Materials, Q-MAT, CESAM, Université de Liège, 4000 Sart Tilman, Belgium*

⁵*Wuhan National High Magnetic Field Center, School of Physics, Huazhong University of Science and Technology, Wuhan 430074, China*

⁶*National University of Science and Technology (MISIS), Moscow 119049, Russia*

⁷*Physics Faculty, Moscow State University, Moscow 119991, Russia*

⁸*National Research South Ural State University, Chelyabinsk 454080, Russia*



(Received 15 January 2018; revised manuscript received 7 March 2018; published 26 March 2018)

We report on magneto-optical imaging and the temperature dependency of the upper critical fields $H_{c2}^c(T)$ parallel to the c axis and $H_{c2}^{ab}(T)$ parallel to the ab plane in $\text{Ba}_2\text{Ti}_2\text{Fe}_2\text{As}_4\text{O}$ single crystals. These data were inferred from the measurements of the temperature-dependent resistance in static magnetic fields up to 14 T and magnetoresistance in pulsed fields up to 60 T. H_{c2} values are found to be 52 and 50 T for $H \parallel ab$ and $H \parallel c$, respectively. These values are 1.2–1.35 times larger than the weak-coupling Pauli paramagnetic limit ($H_p \sim 1.84T_c$), indicating that enhanced paramagnetic limiting is essential and this superconductor is unconventional. Our observations of strong bending in the $H_{c2}^{ab}(T)$ curves and a nearly isotropic maximum upper critical field $H_{c2}^{ab}(0) \approx H_{c2}^c(0)$ support the presence of a strong Pauli paramagnetic effect. We show that the Werthamer-Helfand-Hohenberg (WHH) formula that includes the spin-orbit scattering can effectively describe the $H_{c2}^{ab}(T)$ curve, whereas H_{c2} deviates from the conventional WHH theoretical model without considering the spin paramagnetic effect for the $H \parallel c$ and $H \parallel ab$ directions. For $H \parallel c$, a two-band model is required to fully reproduce the behavior of H_{c2} , while for $H \parallel ab$ the spin paramagnetic effect is responsible for the behavior of H_{c2} . The anisotropy of H_{c2} is close to 3 near T_c and decreases rapidly at lower temperatures.

DOI: [10.1103/PhysRevB.97.115152](https://doi.org/10.1103/PhysRevB.97.115152)

I. INTRODUCTION

The discovery of high-transition-temperature (T_c) superconductivity in iron arsenide-based compounds has triggered a wide interest in the community of condensed-matter physics [1]. With T_c up to 55 K, high critical fields, and moderate anisotropy of their superconducting properties, these compounds show potential for applications [2–4]. As to fundamental research, they offer rich phase diagrams resulting from several competing or cooperative order parameters that have attracted particular attention [5–9]. Furthermore, the multiband nature of iron-based compounds, which are, for the most part, moderately correlated electron systems, adds to their complexity. There are various families of iron-based superconductors, which are named according to their crystal structure [7]. Among them, the so-called 122 family with a ThCr_2Si_2 -type structure ($I4/mmm$) is one of the most studied systems. Superconductivity in the 122 family was first discovered in $(\text{Ba},\text{K})\text{Fe}_2\text{As}_2$ [10] with alkali-metal/alkaline-earth substitution. Subsequently, it was found that superconductivity can also be induced by transition-metal substitutions [11–13] or substitutions on the As site [14].

Recently, a new iron-based oxypnictide superconductor, $\text{Ba}_2\text{Ti}_2\text{Fe}_2\text{As}_4\text{O}$ (Ba22241), was discovered and subjected to an effective self-doping property [15–17]. This offers an alternative and efficient route for inducing superconductivity, instead of achieving it mechanically or chemically via element substitution [18]. The self-doping stems from an interlayer electronic interaction since this compound contains not only the same Fe_2As_2 layers as in other Fe-based superconductors but also another conducting Ti_2O sheet, which makes it very distinctive. For this material, the crystal structure of Ba22241 (represented in Fig. 1) can be viewed as an intergrowth of BaFe_2As_2 and $\text{BaTi}_2\text{As}_2\text{O}$, containing not only superconducting Fe_2As_2 layers but also conducting Ti_2O sheets. In $\text{BaTi}_2\text{As}_2\text{O}$, the Ti_2O sheets undergo a possible charge/spin density wave (CDW/SDW) transition around 200 K [15,19], while in Ba22241, the CDW/SDW transition occurs at 125 K. Although neither BaFe_2As_2 nor $\text{BaTi}_2\text{As}_2\text{O}$ is superconducting, the combined structure, Ba22241, shows superconductivity without doping. Based on the variation of the bond-valence sum of Ti, electron transfer from Ti to Fe was proposed to interpret the appearance of superconductivity as a result of self-doping [15].

The upper critical field H_{c2} is one of the fundamental parameters in type-II superconductors, which provides valuable information on the microscopic origin of pair breaking and reflects the electronic structure responsible for

*mahmoudhafiez@gmail.com

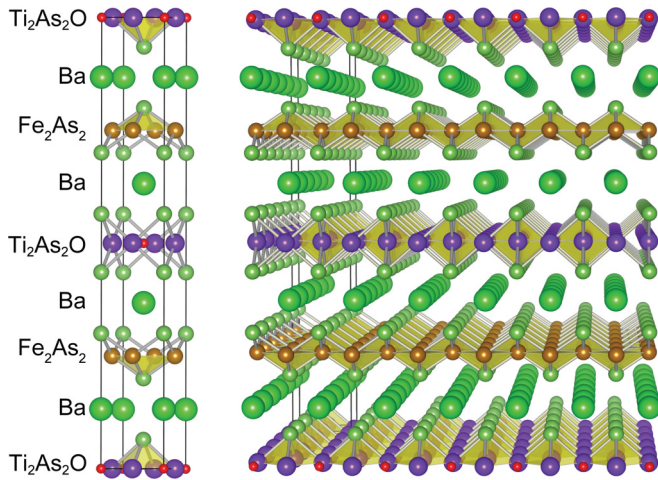


FIG. 1. The crystal structure of $\text{Ba}_2\text{Ti}_2\text{Fe}_2\text{As}_4\text{O}$ (Ba22241) is an intergrowth of BaFe_2As_2 and $\text{BaTi}_2\text{As}_2\text{O}$. One can see blocks of Fe_2As_2 , Ba, and $\text{Ti}_2\text{As}_2\text{O}$ are stacked along the c axis of the tetragonal cell, which makes this layered crystal structure belong to the $I4/mmm$ space group.

superconductivity. Additionally, the anisotropy of H_{c2} , which is related to the dimensionality and the topology of the underlying electronic structure, also becomes important for potential applications as well as for understanding multiband effects [20]. Fe-based superconductors usually possess an extremely large $H_{c2}(T)$, limiting its determination to temperatures near T_c , giving rise to inaccurate extrapolations of $H_{c2}(0)$. Therefore, large magnetic fields are required to study $H_{c2}(T)$ of the Fe-based superconductors. The recently discovered Ba22241 is expected to have very high upper critical fields $H_{c2}(T)$ mediated by the interplay of multiband orbital effects and strong Pauli pair breaking, characteristic of Fe-based superconductors.

To the best of our knowledge, there are no reports of the anisotropy of $H_{c2}(T)$ in the conducting plane of Ba22241 or hints as to whether it would be different from that of the well-studied 122 Fe-based [21,22]. Another important question is whether multiband superconductivity in ordered Ba22241 could result in crossing of the H_{c2} curves, as observed in some Fe-based superconductors and other superconductors [23–25]. In an attempt to address these issues, in this paper we present measurements of anisotropic magnetoresistance and $H_{c2}(T)$ anisotropy in Ba22241 single crystals in high magnetic fields up to 60 T. We found that the system shows a nearly isotropic $H_{c2}(0)$ and strongly nonlinear $H_{c2}^{ab}(T)$. The details of the temperature dependence of H_{c2} curves can be successfully accounted for in the Werthamer-Helfand-Hohenberg (WHH) model. Our results suggest that the Pauli-limiting effect could be the main source of the peculiar isotropic $H_{c2}(0)$ for this Ba22241 superconductor.

II. EXPERIMENT

A FeAs-flux method is efficient for growing oxygen-free crystals [26,27], such as those of the 122 system, but not for oxyphnictides such as Ba22241 [16]. High-quality single crystals of Ba22241 were grown out of Ba_2As_3 flux at ambient

pressure [16]. Due to the toxicity of arsenic, all procedures related to the sample preparation were performed in a glove box. The flux, with nominal compositions of Ba_2As_3 , was prepared by reacting Ba and As in a sealed quartz tube. Following Ref. [16], batches with platelet-like single crystals with an area of $(2.5 \times 2.5) \text{ mm}^2$ and masses up to 3 mg were carefully examined by electron probe microanalyzer and x-ray powder diffraction.

The visualization of the magnetic flux landscape was performed through the Faraday rotation of linearly polarized light in a Bi-doped yttrium iron garnet with in-plane magnetic domains, a technique known as magneto-optical imaging (MOI) [28,29]. Details of the sample mounting, image acquisition, and postimage processing can be found in Ref. [30]. This technique requires planar surfaces to achieve the best results, as the resolution is strongly dependent on the proximity of the magneto-optical indicator to the sample. To that end, we cleaved large single crystals using a traditional Scotch-tape method on both sides, thus obtaining flat samples of millimeter-scale length. Samples used for four-probe electrical resistivity measurements were cleaved from the inner parts of large single crystals (with surface area up to 1 cm^2 and 0.3 mm thickness) and had dimensions of typically $(2-3) \times 0.5 \times 0.1 \text{ mm}^3$. Both DuPont 4929N silver paint and Epotek-H20E silver epoxy were used to attach contact leads onto the samples (Pt for static field measurements). In order to determine the field dependence of H_{c2} near T_c more accurately, the temperature dependence was measured with a Quantum Design (QD) physical property measurement system (PPMS) with magnetic fields up to 14 T. Finally, to ensure low noise during the measurements, all Ohmic contacts, made of silver epoxy, had resistances of less than 1Ω . The upper critical field H_{c2} at low temperature was measured in a 60 T pulsed magnet at the Wuhan National High Magnetic Field Center. The resistance was measured with a standard four-probe method with an excitation current of 5 mA at a frequency of $\sim 70 \text{ kHz}$. A high-speed data acquisition card recorded the reference voltage of the current and the sample voltage at a rate of 3 MHz. The data were then extracted by software with a phase-locked method.

III. RESULTS AND DISCUSSION

A. Magneto-optical imaging

Figure 2 illustrates the results obtained by MOI of the Ba22241 sample. In the top left corner, the optical image of the sample shows the irregularities in the surface height, as well as a hole through the material. The image in the bottom right inset shows the magnetic flux distribution in the superconducting state at 3.6 K and $H = 0 \text{ mT}$, after field cooling the sample in an out-of-plane magnetic field $H = 1 \text{ mT}$. Even though the field is weak, the flux penetration in the sample is significant, namely, close to the hole. Moreover, we see that the penetration is rather inhomogeneous since some sites at the borders clearly show enhanced penetration. The determination of the critical temperature was also done by MOI, as represented in the main graph in Fig. 2. In order to do this, we started from the remnant state represented in the bottom right inset, and we tracked the intensity I averaged over a $15 \times 15 \mu\text{m}^2$ square while

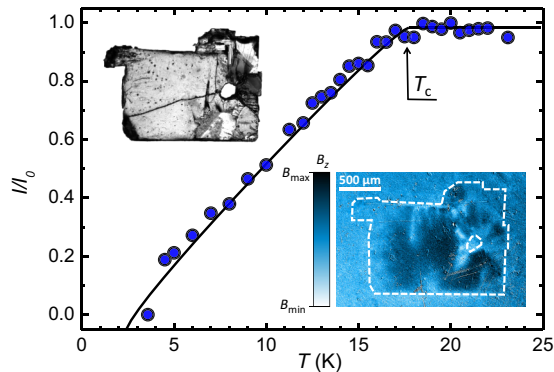


FIG. 2. Superconducting-to-normal-state transition of a Ba₂Ti₂Fe₂As₄O (Ba22241) sample obtained by magneto-optical imaging (MOI). A bright-field optical microscopy image of the sample surface is shown in the top left inset. The sample was cooled down to $T = 3.6$ K in an out-of-plane magnetic field $H = 1$ mT. The inset in the bottom right corner shows the magnetic field distribution after setting $H = 0$ mT. Bright (dark) areas correspond to low (high) magnetic fields; B_{\max} (B_{\min}) is approximately 1 mT (-0.2 mT). The temperature was subsequently increased, and the critical temperature T_c was determined by tracking the average intensity I in a $15 \times 15 \mu\text{m}^2$ square at the center of the sample. I is normalized by the intensity I_0 outside the sample.

gradually increasing the temperature. The data represented in the graph are normalized by the intensity I_0 measured outside the sample. From these measurements, we estimated a critical temperature $T_c = 17.5 \pm 1$ K, which is similar to the specific-heat data (not shown). In addition, T_c estimated by magnetization measurements (like MOI) is systematically lower than that obtained from electrical transport (see below) due to the nature of the measurements. However, since the stepped sample surface made it difficult to have the indicator in close proximity to the whole sample surface, this value should be considered with some caution. Indeed, the actual T_c could be slightly underestimated since the magnetic signal, weakened when the indicator-to-sample gap is increased [31], could be buried in noise before the transition to the normal state takes place.

B. Transport properties

Figure 3 summarizes the temperature dependence of the in-plane electrical resistivity at different applied fields. The criteria for determining T_c are shown in Fig. 3(a). The onset criterion identifies the temperature at which the normal-state line intersects the maximum slope of the resistance curve. The offset criterion identifies the temperature of the intersection of the maximum slope of the resistance curve and the zero-resistance line. In zero field, the superconducting transition is rather sharp, with $\Delta T \sim T_{\text{onset}} - T_{\text{offset}} \sim 2.3$ K. The residual resistivity ratio (RRR) is found to be $\rho_{300\text{K}}/\rho_{25\text{K}} \sim 1.6$. Under a magnetic field of 14 T, the superconducting transition is broadened and shifted significantly to lower temperatures. For $H \parallel c$, the T_c values are more significantly suppressed than for $H \parallel ab$ at a given field, likely the result of enhanced thermally activated vortex motion in this direction [32]. Similar field broadening of resistivity after applying magnetic field

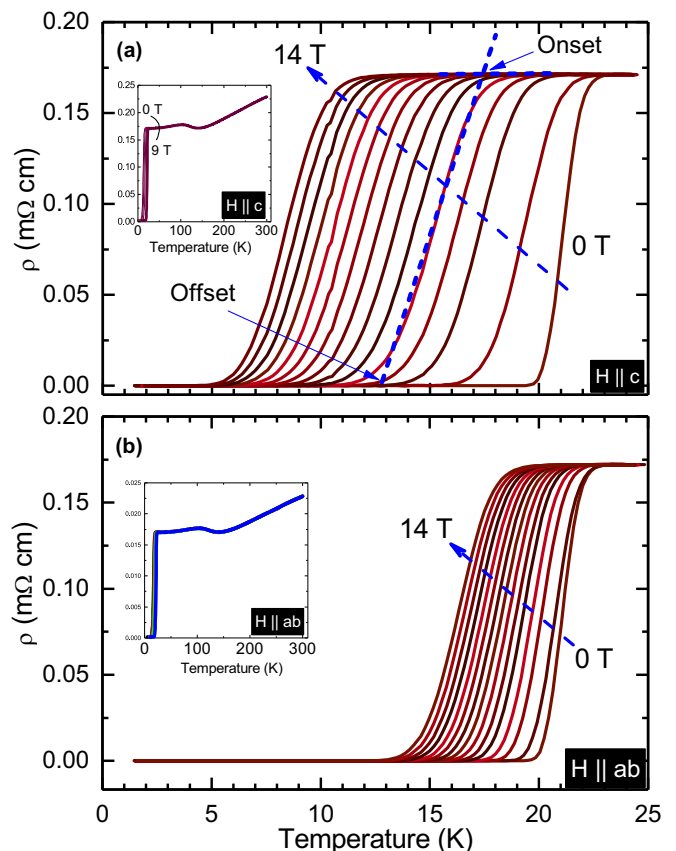


FIG. 3. Temperature-dependent resistance measured in a QD PPMS at different applied fields with (a) $H \parallel c$ and (b) $H \parallel ab$. The dashed line and arrows indicate different criteria for determining H_{c2} (see text). The insets illustrate the temperature dependence of the in-plane resistance measurements upon heating of Ba22241 up to 300 K.

is explained by the vortex-liquid state in NdFeAsO_{1-x}F_x single crystals [33,34]. However, it is rather different from 1111 systems such as single crystals of SmO_{0.7}FeAs and SmO_{0.85}FeAs [35,36]. Obviously, the resistivity upturn at $T_{CDW/SDW} \approx 120$ K, shown in the insets of Fig. 3, correlates with a possible CDW or SDW transition in the Ti₂As₂O layers in the original study [15]. The nature of this upturn in the resistivity remains mysterious because both Fe and Ti sublattices could play a role. However, this upturn was tentatively ascribed by Raman scattering and optical spectroscopy studies to a possible density-wave transition in the Ti sublattice [37,38]. Very recently, inelastic neutron scattering indicated the absence of any magnetic effect in Ba22241 [18]. Furthermore, Mössbauer measurements did not evidence the occurrence of any long-range magnetic ordering below the $T = 125$ K originating from the Fe sublattice in Ba22241 [18]. The transitions in the Ba22241 system are consistent with the values obtained from previous reports [15]. The normal-state resistivity presents a semiconductor-like behavior at low temperatures, indicating that there is still some Ti occupation in the Fe plane.

Figure 4 summarizes the isothermal magnetic field sweep resistance data taken at different temperatures in magnetic

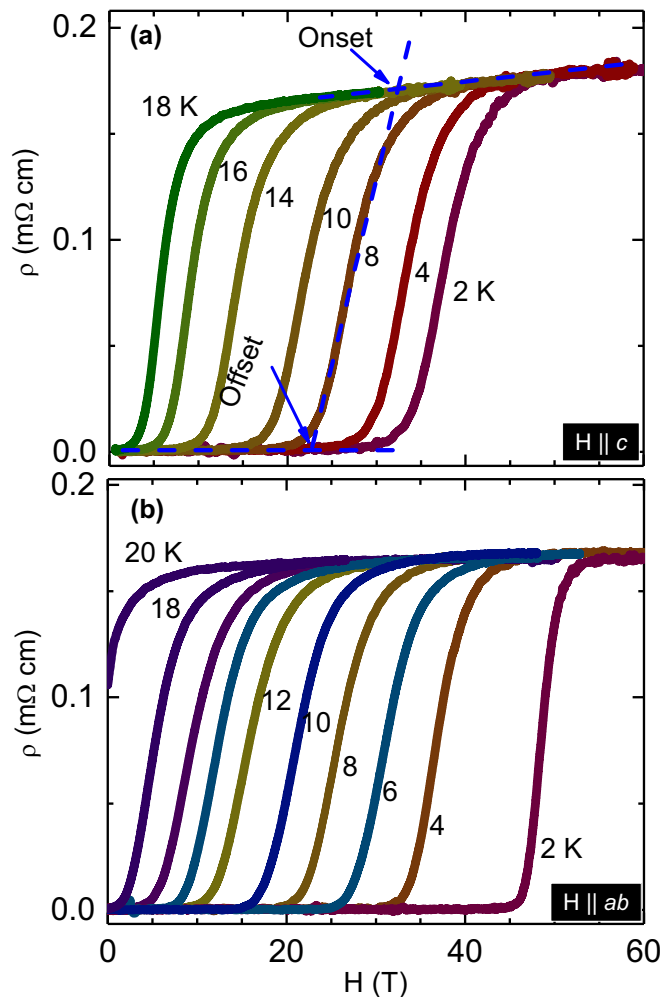


FIG. 4. Field-dependent resistance measured in a 60-T pulsed magnet at different temperatures with (a) $H \parallel ab$ and (b) $H \parallel c$. The dashed line and arrows indicate different criteria for determining H_{c2} .

fields aligned along the c axis [Fig. 4(a)] and along the direction of the conducting plane [Fig. 4(b)] in Ba22241. At $H > 14$ T, the transition into the superconducting state for $H \parallel ab$ occurs at higher temperatures than for $H \parallel c$, indicating that $H_{c2}^{ab}(T)$ is higher than $H_{c2}^c(T)$ at temperatures near T_c . Onset and offset criteria similar to those in Fig. 3(a) were applied to extract the superconducting field values at a given temperature [presented in Fig. 4(a)].

One of the mechanisms that determines the upper critical field of superconductors is related to the supercurrent flow screening the magnetic field and is referred to as orbital limiting and described by the WHH theory [39]. However, in some materials the upper critical field is not determined by the orbital limiting. This scenario can be found in materials where the orbital motion of electrons is hampered by either a short mean free path, heavy mass of conduction electrons in heavy-fermion materials, or weak links between the conducting layers in Josephson structures or in naturally highly electronically anisotropic layered materials [40], provided that the magnetic field is aligned parallel to the conducting layer. Figure 5 illustrates the anisotropic $H_{c2}(T)$ data inferred from the temperature-dependent and field-dependent

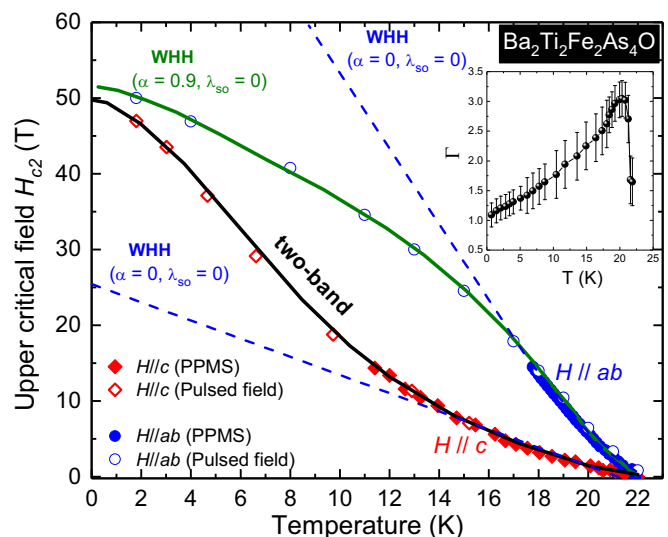


FIG. 5. Phase diagram of H_{c2} vs temperature of Ba22241 up to 60 T for the field applied parallel and perpendicular to c . T_c has been estimated through the onset values as explained in the text. Solid symbols (from the PPMS) and open symbols (from the pulsed magnet) represent H_{c2} for $H \parallel ab$ in blue and H_{c2} for $H \parallel c$ in red. The inset shows the anisotropy $\Gamma = H_{c2}^{B/Lc} / H_{c2}^{B/Lc}$ determined from an interpolation of the H_{c2} curves.

resistance data. $H_{c2}(T)$ clearly shows a different behavior depending on the direction of H . The curve of H_{c2} for $H \parallel ab$ has a tendency to saturate with decreasing temperature, while H_{c2} for $H \parallel c$ presents a curvature near 0 K without saturation. In fact, superconductivity can be suppressed either by orbital pair breaking of Cooper pairs in the superconducting state (as described above) or with a spin effect due to Zeeman splitting which applies only to the singlet pairings and limits superconductivity below a certain value known as the Clogston-Chandrasekhar [41] paramagnetic limit. This field is determined by a decrease in paramagnetic energy, which becomes equal to the condensation energy of the superconductor. In weak-coupling BCS superconductors, the paramagnetic-limiting field is determined in the $T \rightarrow 0$ limit as $H_p = 1.8T_c$. Note, however, that even in materials with dominant paramagnetic effects, the behavior of $H_{c2}(T)$ close to zero-field T_c is always determined by the orbital-limiting mechanism, so that the slope of H_{c2} lines at T_c reflects the anisotropy of the electronic structure. The width of the temperature range in which the orbital-limiting mechanism is dominant depends on the ratio of orbital- and paramagnetic-limiting fields (the Maki parameter) [42]. The temperature dependence of H_{c2} is given by the WHH formula:

$$\ln \frac{1}{t} = \sum_{\nu=-\infty}^{\infty} \frac{1}{2\nu+1} - \left[2\nu+1 + \frac{\bar{h}}{t} + \frac{(\frac{\alpha\bar{h}}{t})^2}{2\nu+1 + \frac{\bar{h}+\lambda_{so}}{t}} \right]^{-1}, \quad (1)$$

where $t = T/T_c$, $\bar{h} = (4/\pi^2)[H_{c2}(T)/|dH_{c2}/dT|_{T_c}]$, α is the Maki parameter which describes the relative strength of orbital breaking and the limit of paramagnetism, and λ_{so} is the

spin-orbit scattering constant [39]. The orbital-limiting field H_{c2}^{orb} at zero temperature is determined by the slope at T_c as $H_{c2}^{\text{orb}} = 0.69 T_c (\partial H_{c2}/\partial T)|_{T_c}$. A fit to the H_{c2}^{ab} data in the whole measurement range for spin-paramagnetic effects ($\alpha = 0.9$) and negligible spin-orbit scattering ($\lambda_{so} = 0$) yields a critical field of 52 T. However, H_{c2} for both configurations deviates from the conventional WHH theoretical model without considering the spin-paramagnetic effect and spin-orbit scattering. The dashed lines in Fig. 5 are the best fits of the WHH model to the data, assuming negligible spin-orbit coupling. The corresponding theoretical curves $H_{c2}(T)$ are shown in Fig. 5. In reality, paramagnetic and spin-orbit effects are expected to play a role. However, a fit to the data including α and λ_{so} as free parameters is reasonable in our case due to the limited field range of investigation. For the configuration with $H \parallel c$, we used a different approach: An independent estimate for α is obtained from the orbital-limiting field $\mu_0 H_{c2}^{\text{orb}}$ and the Pauli-limiting field $H_{c2}^{\text{P}} = \Delta_0/1.41\mu_B$. When $\lambda_{so} = 0$, $H_{c2}(0)$ can be obtained from the WHH formula following the relation

$$\alpha = \sqrt{2}H_{c2}^{\text{orb}}/H_{c2}^{\text{P}}. \quad (2)$$

Here, the Pauli-limiting field can be estimated by $H_p^{BCS}(T = 0) = 1.84(H = 0)$ for isotropic s -wave pairing in the absence of spin-orbit scattering. In our case, $H_p^{BCS} = 40$ T, which is 1.4 times this limit, indicating that the Zeeman paramagnetic pair breaking may be essential for H_{c2}^c . It is common for the weak-coupling BCS formula to underestimate the actual paramagnetic limit. Consequently, we expect for in-plane fields pronounced Pauli-limiting effects leading to a curvature change of the H_{c2}^{ab} data with saturation towards zero temperature. This indeed agrees well with our observation. We noticed that the BCS estimate of the Pauli limit where $H_p = 1.84T_c$ might underestimate the Pauli limit. A more precise determination may be obtained from $H_p(0) = \Delta_0/\sqrt{2}\mu_B$. For this, $\Delta_0/k_B T_c$ could be obtained from the heat-capacity anomaly at T_c in zero field. Preliminary attempts to identify this anomaly from heat-capacity measurements were inconclusive, and further experiments are needed to explore this point.

Previously, several reports on $H_{c2}(T)$ in Fe-based superconductors have shown that a two-band model in combination with orbital-limiting effects can effectively describe the overall curvature of $H_{c2}(T)$ [35,43–45]. The main motivation for invoking the two-band model is to explain the almost linear or sublinear increase in the concave shape of the $H_{c2}(T)$ curve near T_c and its change to a convex form with decreasing temperature. It is expected that the Pauli limit will be quite effective in explaining the isotropic H_{c2}^0 , while the orbital effect can explain the anisotropy near T_c between the H_{c2}^{ab} and H_{c2}^c curves [46,47]. Although the low-temperature (0 K) upper critical field is rather isotropic, the initial slope near T_c does clearly show a dependence on the field orientation (Fig. 5), perhaps resulting from details of the vortex structure, the Fermi-surface topology, or different sample edge properties.

On the other hand, H_{c2}^c shows a curvature near $T \sim 0$ K without saturation. We consider that the residual upward curvature of $H_{c2}^c(T)$ originates from two-band features recently shown by various experiments with iron arsenide compounds [45]. With

this motivation, we attempted to fit the experimental $H_{c2}(T)$ curves with the effective two-band model [48]. In the dirty limit, the equation for the two-band BCS model with orbital pair breaking and negligible interband scattering is

$$a_0[\ln t + U(h)][\ln t + U(\eta h)] + a_2[\ln t + U(\eta h)] + a_1[\ln t + U(h)] = 0, \quad (3)$$

$$U(x) = \psi(1/2 + x) - \psi(1/2), \quad (4)$$

where $\psi(x)$ is the digamma function, $a_0 = 2(\lambda_{11}\lambda_{22} - \lambda_{12}\lambda_{21})/\lambda_0$, $a_1 = 1 + (\lambda_{11} - \lambda_{22})/\lambda_0$, $a_2 = 1 - (\lambda_{11} - \lambda_{22})/\lambda_0$, $\lambda_0 = \sqrt{(\lambda_{11}^2 - \lambda_{22}^2)^2 + 4\lambda_{12}\lambda_{21}}$, and $\eta = \frac{D_2}{D_1}$. Hence, there are in total six free parameters in the fitting process, λ_{11} , λ_{22} , λ_{12} , λ_{21} , D_1 , and η . We use $a_0 = 1$, $a_1 = 1.5$, and $a_2 = 0.5$, i.e., the same values as for the BaFe_{2-x}Ni_xAs₂ superconductors [49]. The best fit with $D_1 = 4.9$ and $\eta = 0.36$ agrees very well with the H_{c2}^c data and gives $H_{c2}^c \approx 49$ T. One has to notice that it is also possible to fit the H_{c2}^{ab} data with the two-band model, but that would introduce a much higher uncertainty in the obtained parameters because of the additional parameters to be used.

To discuss the anisotropy of the upper critical field, we have plotted the values of H_{c2} vs T for the different field orientations in the inset of Fig. 5. We calculated the anisotropy $\Gamma = H_{c2}^{\text{ab}}/H_{c2}^c$ using a point-by-point interpolation. The anisotropy monotonically decreases with decreasing temperature and reaches about 1 for zero temperature. This feature is in line with the widely observed reduction of the anisotropy as the temperature decreases [50]. Additionally, this weakened anisotropy at low temperatures, also observed in many other Fe-based superconductors, is a consequence of the Pauli-limiting effect that quickly becomes dominant for H_{c2}^{ab} somewhat below T_c . Therefore, the temperature dependence of the anisotropy originates from the combined effect of the two-band nature and spin paramagnetism. This distinguishes Ba22241 from other ordered stoichiometric Fe-based compounds like LiFeAs for which the entire anisotropic $H_{c2}(T)$ has been measured [51]. It should be noted that the trend of the anisotropy value reported here has been observed in all iron-based superconductors [50]. The origin of the small anisotropy of the upper critical fields could be caused by a three-dimensional electronic structure, spin paramagnetism, or multiband effects [50].

Finally, as can be seen from Fig. 5, the upper critical fields for both crystallographic orientations are higher than the weak-limit paramagnetic limiting $H_p \approx 40$ T. These high values may come from the strong-coupling nature of superconductivity in iron pnictides or, indeed, reflect paramagnetic limiting at low temperatures, as was suggested in several studies [51,52].

IV. CONCLUSION

In summary, we have determined the $H_{c2}(T)$ phase diagram for Ba22241 from electrical-transport measurements in magnetic fields up to 60 T aligned both within the ab plane and along the c axis. The behavior for $H \parallel c$ can be described by an effective two-band model, whereas the $H \parallel ab$ data

follow the WHH model including orbital pair-breaking and spin-paramagnetic effects. The anisotropy Γ of the critical field is largest close to T_c and monotonically decreases from about 3 near T_c to 1 at 0 K due to the strong paramagnetic pair-breaking effects for in-plane magnetic fields. The presence of the Maki parameter α describing the Pauli-limiting effect in the WHH scheme is essential to describe much smaller H_{c2} values than were expected for the orbital-limiting field. Therefore, the Pauli limiting is postulated to be a dominant mechanism in determining the nearly isotropic H_{c2} behavior because the Zeeman splitting energy should be able to break the singlet Cooper pair in an isotropic manner regardless of the details of the electronic structure.

ACKNOWLEDGMENTS

We are grateful to the support of the Deutsche Forschungsgemeinschaft (DFG) through MO 3014/1-1. A.V.S. and J.B. acknowledge support from ARC Grant No. 13/18-08 for Concerted Research Actions, financed by the French Community of Belgium (Wallonia-Brussels Federation). A.N.V. acknowledge support from Russian Foundation for Basic Research grant 17-29-10007. This work was supported by the Ministry of Education and Science of the Russian Federation in the framework of Increase Competitiveness Program of NUST (MISiS) Grant No. K2-2017-084, by act 211 of the government of the Russian Federation, Contracts No. 02.A03.21.0004 and 02.A03.21.0011.

- [1] Y. Kamihara, T. Watanabe, M. Hirano, and H. Hosono, *J. Am. Chem. Soc.* **130**, 3296 (2008).
- [2] M. Putti, I. Pallecchi, E. Bellingeri, M. R. Cimberle, M. Tropeano, C. Ferdeghini, A. Palenzona, C. Tarantini, A. Yamamoto, J. Jiang, J. Jaroszynski, F. Kametani, D. Abramov, A. Polyanskii, J. D. Weiss, E. E. Hellstrom, A. Gurevich, D. C. Larbalestier, R. Jin, B. C. Sales, A. S. Sefat, M. A. McGuire, D. Mandrus, P. Cheng, Y. Jia, H. H. Wen, S. Lee, and C. B. Eom, *Supercond. Sci. Technol.* **23**, 034003 (2010).
- [3] K. Tanabe and H. Hosono, *Jpn. J. Appl. Phys.* **51**, 010005 (2012).
- [4] J.-i. Shimoyama, *Supercond. Sci. Technol.* **27**, 044002 (2014).
- [5] J. Paglione and R. L. Greene, *Nat. Phys.* **6**, 645 (2010).
- [6] D. C. Johnston, *Adv. Phys.* **59**, 803 (2010).
- [7] G. R. Stewart, *Rev. Mod. Phys.* **83**, 1589 (2011).
- [8] M. Abdel-Hafiez, Y. J. Pu, J. Brisbois, R. Peng, D. L. Feng, D. A. Chareev, A. V. Silhanek, C. Krellner, A. N. Vasiliev, and X.-J. Chen, *Phys. Rev. B* **93**, 224508 (2016).
- [9] M. Abdel-Hafiez, Y. Zhang, Z. He, J. Zhao, C. Bergmann, C. Krellner, C.-G. Duan, X. Lu, H. Luo, P. Dai, and X.-J. Chen, *Phys. Rev. B* **91**, 024510 (2015).
- [10] M. Rotter, M. Tegel, and D. Johrendt, *Phys. Rev. Lett.* **101**, 107006 (2008).
- [11] A. S. Sefat, R. Jin, M. A. McGuire, B. C. Sales, D. J. Singh, and D. Mandrus, *Phys. Rev. Lett.* **101**, 117004 (2008).
- [12] N. Ni, M. E. Tillman, J.-Q. Yan, A. Kracher, S. T. Hannahs, S. L. Bud'ko, and P. C. Canfield, *Phys. Rev. B* **78**, 214515 (2008).
- [13] P. C. Canfield and S. L. Bud'ko, *Annu. Rev. Condens. Matter Phys.* **1**, 27 (2010).
- [14] S. Jiang, H. Xing, G. Xuan, C. Wang, Z. Ren, C. Feng, J. Dai, Z. Xu, and G. Cao, *J. Phys.: Condens. Matter* **21**, 382203 (2009).
- [15] Y. L. Sun, J. Hao, H. F. Zhai, J. K. Bao, W. H. Jiao, Q. Tao, C. Y. Shen, Y. W. Zeng, Z. A. Xu, and G. H. Cao, *J. Am. Chem. Soc.* **134**, 12893 (2012).
- [16] Y. L. Sun, A. Ablimit, J. K. Bao, H. Jiang, J. Zhou, and G. H. Cao, *Sci. Technol. Adv. Mater.* **14**, 055008 (2013).
- [17] J.-Z. Ma, A. van Roekeghem, P. Richard, Z.-H. Liu, H. Miao, L.-K. Zeng, N. Xu, M. Shi, C. Cao, J.-B. He, G.-F. Chen, Y.-L. Sun, G.-H. Cao, S.-C. Wang, S. Biermann, T. Qian, and H. Ding, *Phys. Rev. Lett.* **113**, 266407 (2014).
- [18] M. Zbiri, W. Jin, Y. Xiao, Y. Sun, Y. Su, S. Demirdis, and G. Cao, *Phys. Rev. B* **95**, 174301 (2017).
- [19] X. F. Wang, Y. J. Yan, J. J. Ying, Q. J. Li, M. Zhang, N. Xu, and X. H. Chen, *J. Phys.: Condens. Matter* **22**, 075702 (2012).
- [20] X. Xing, W. Zhou, J. Wang, Z. Zhu, Y. Zhang, N. Zhou, B. Qian, X. Xu, and Z. Shi, *Sci. Rep.* **7**, 45943 (2017).
- [21] M. Kano, Y. Kohama, D. Graf, F. Balakirev, A. S. Sefat, M. A. McGuire, B. C. Sales, D. Mandrus, and S. W. Tozer, *J. Phys. Soc. Jpn.* **78**, 084719 (2009).
- [22] C. Tarantini, A. Gurevich, J. Jaroszynski, F. Balakirev, E. Bellingeri, I. Pallecchi, C. Ferdeghini, B. Shen, H. H. Wen, and D. C. Larbalestier, *Phys. Rev. B* **84**, 184522 (2011).
- [23] M. Fang, J. Yang, F. F. Balakirev, Y. Kohama, J. Singleton, B. Qian, Z. Q. Mao, H. Wang, and H. Q. Yuan, *Phys. Rev. B* **81**, 020509 (2010).
- [24] B. Maiorov, P. Mele, S. A. Baily, M. Weigand, S.-Z. Lin, F. F. Balakirev, K. Matsumoto, H. Nagayoshi, S. Fujita, Y. Yoshida, Y. Ichino, T. Kiss, A. Ichinose, M. Mukaida, and L. Civale, *Supercond. Sci. Technol.* **27**, 044005 (2014).
- [25] F. F. Balakirev, T. Kong, M. Jaime, R. D. McDonald, C. H. Mielke, A. Gurevich, P. C. Canfield, and S. L. Bud'ko, *Phys. Rev. B* **91**, 220505 (2015).
- [26] X. F. Wang, T. Wu, G. Wu, H. Chen, Y. L. Xie, J. J. Ying, Y. J. Yan, R. H. Liu, and X.-H. Chen, *Phys. Rev. Lett.* **102**, 117005 (2009).
- [27] P. C. Canfield, S. L. Bud'ko, N. Ni, J. Q. Yan, and A. Kracher, *Phys. Rev. B* **80**, 060501 (2009).
- [28] C. Jooss, J. Albrecht, H. Kuhn, S. Leonhardt, and H. Kronmüller, *Rep. Prog. Phys.* **65**, 651 (2002).
- [29] M. R. Koblischka and R. J. Wijngaarden, *Supercond. Sci. Technol.* **8**, 199 (1995).
- [30] J. Brisbois, O. A. Adami, J. I. Avila, M. Motta, W. A. Ortiz, N. D. Nguyen, P. Vanderbemden, B. Vanderheyden, R. B. G. Kramer, and A. V. Silhanek, *Phys. Rev. B* **93**, 054521 (2016).
- [31] G. Shaw, J. Brisbois, L. B. G. L. Pinheiro, J. Müller, S. Blanco Alvarez, T. Devillers, N. M. Dempsey, J. E. Scheerder, J. Van de Vondel, S. Melinte, P. Vanderbemden, M. Motta, W. A. Ortiz, K. Hasselbach, R. B. G. Kramer, and A. V. Silhanek, *Rev. Sci. Instrum.* **89**, 023705 (2018).
- [32] H.-J. Kim, Y. Liu, Y. S. Oh, S. Khim, I. Kim, G. R. Stewart, and K. H. Kim, *Phys. Rev. B* **79**, 014514 (2009).
- [33] Z. Pribulova, T. Klein, J. Kacmarcik, C. Marcenat, M. Konczykowski, S. L. Bud'ko, M. Tillman, and P. C. Canfield, *Phys. Rev. B* **79**, 020508(R) (2009).
- [34] A. Adamski, C. Krellner, and M. Abdel-Hafiez, *Phys. Rev. B* **96**, 100503(R) (2017).

- [35] H.-S. Lee, M. Bartkowiak, J.-H. Park, J.-Y. Lee, J.-Y. Kim, N.-H. Sung, B. K. Cho, C.-U. Jung, J. S. Kim, and H.-J. Lee, *Phys. Rev. B* **80**, 144512 (2009).
- [36] J. Karpinski, N. D. Zhigadlo, S. Katrych, Z. Bukowski, P. Moll, S. Weyeneth, H. Keller, R. Puzniak, M. Tortello, D. Daghero, R. Gonnelli, I. Maggio-Aprile, Y. Fasano, Ø. Fischer, K. Rogacki, and B. Batlogg, *Phys. C (Amsterdam, Neth.)* **469**, 370 (2009).
- [37] S. F. Wu, P. Richard, W. L. Zhang, C. S. Lian, Y. L. Sun, G. H. Cao, J. T. Wang, and H. Ding, *Phys. Rev. B* **89**, 134522 (2014).
- [38] M. Zbiri, R. Mittal, S. Rols, Y. Su, Y. Xiao, H. Schober, S. L. Chaplot, M. Johnson, T. Chatterji, Y. Inoue, S. Matsuishi, H. Hosono, and Th. Brueckel, *J. Phys.: Condens. Matter* **22**, 315701 (2010).
- [39] N. R. Werthamer, E. Helfand, and P. C. Hohenberg, *Phys. Rev.* **147**, 295 (1966).
- [40] T. Ishiguro, *J. Supercond.* **13**, 817 (2000).
- [41] A. M. Clogston, *Phys. Rev. Lett.* **9**, 266 (1962).
- [42] K. Maki, *Phys. Rev.* **148**, 362 (1966).
- [43] J. Jaroszynski, F. Hunte, L. Balicas, Y.-j. Jo, I. Raičević, A. Gurevich, D. C. Larbalestier, F. F. Balakirev, L. Fang, P. Cheng, Y. Jia, and H. H. Wen, *Phys. Rev. B* **78**, 174523 (2008).
- [44] S. A. Baily, Y. Kohama, H. Hiramatsu, B. Maiorov, F. F. Balakirev, M. Hirano, and H. Hosono, *Phys. Rev. Lett.* **102**, 117004 (2009).
- [45] F. Hunte, J. Jaroszynski, A. Gurevich, D. Larbalestier, R. Jin, S. A. Sefat, M. A. McGuire, B. C. Sales, D. K. Christen, and D. Mandrus, *Nature (London)* **453**, 903 (2008).
- [46] D. A. Zocco, K. Grube, F. Eilers, T. Wolf, and H. V. Löhneysen, *Phys. Rev. Lett.* **111**, 057007 (2013).
- [47] C.-w. Cho, J. H. Yang, N. F. Q. Yuan, J. Shen, T. Wolf, and R. Lortz, *Phys. Rev. Lett.* **119**, 217002 (2017).
- [48] A. Gurevich, *Phys. Rev. B* **67**, 184515 (2003).
- [49] Z. Wang, T. Xie, E. Kampert, T. Förster, X. Lu, R. Zhang, D. Gong, S. Li, T. Herrmannsdörfer, J. Wosnitza, and H. Luo, *Phys. Rev. B* **92**, 174509 (2015).
- [50] J.-L. Zhang, L. Jiao, Y. Chen, and H. Yuan, *Front. Phys.* **6**, 463 (2011).
- [51] K. Cho, H. Kim, M. A. Tanatar, Y. J. Song, Y. S. Kwon, W. A. Coniglio, C. C. Agosta, A. Gurevich, and R. Prozorov, *Phys. Rev. B* **83**, 060502 (2011).
- [52] J. Murphy, M. A. Tanatar, D. Graf, J. S. Brooks, S. L. Bud'ko, P. C. Canfield, V. G. Kogan, and R. Prozorov, *Phys. Rev. B* **87**, 094505 (2013).